Voltage–current characteristics of low pressure discharges in vapors of several alcohols

Journal of Applied Physics

VOLTAGE-CURRENT CHARACTERISTICS OF LOW-PRESSURE DISCHARGES IN VAPOURS OF SEVERAL ALCOHOLS

Jelena Marjanović[1], Dragana Marić[1], Gordana Malović[1] and Zoran Lj. Petrović[2,3]

[1] Institute of Physics Belgrade, University of Belgrade, Pregrevica 118, 11080 Belgrade, Serbia
[2] School of Engineering, Ulster University, Jordanstown, Co. Antrim, BT37 0QB UK
[3] Serbian Academy for Sciences and Arts, Knez Mihailova 35, 11001 Belgrade, Serba

e-mail: z.petrovic@ulster.ac.uk

Abstract. In this paper, we present the results for voltage-current (*V-i*) characteristics of dc low-pressure low to moderate current discharges in vapours of alcohols: methanol, ethanol, isopropanol, and n-butanol vapours. These electrical measurements are supported by optical recordings of axial emission profiles from low-current to high-current regimes. The voltage-current characteristics and the corresponding distribution of emission intensities were typically recorded for two *pd* values, in the left-hand branch of the Paschen curve (0.15 Torr cm) and in the minimum of the Paschen curves (ranging from 0.30 Torr cm to 0.40 Torr cm for different alcohols selected here). In the recorded *V-i* characteristics the different discharge regimes of discharge operation are easily distinguished. Axial profiles of emitted light from the low-current to high-current regimes reveal that heavy particles make up a significant contribution to excitation part in alcohol vapours discharges. In the region of transition from normal to abnormal glow in methanol vapour discharge, sudden changes of the regime of operation were observed and several diagnostic techniques have been applied to them.

1 Introduction

Plasmas that operate in liquids and close to the gas-liquid interface have received a lot of attention in the past 10 years [1]. First, they have a wide range of applications for nanoparticle synthesis, organic compounds decomposition, sterilization, water treatment, etc all the way to biomedical applications even including medical procedures. In addition to discharges associated with liquid water and its vapour, for several years there has been an increasing interest in non-equilibrium discharges in alcohols and their vapours. Fast development of technology and industry imposes the need for such studies both from the fundamental point of view (elementary data, understanding of the main processes and phenomenology, the ability to represent transport in the presence of polar molecules, etc.) and also having in mind targeted applications where the most important examples are production of environmentally responsible fuels and production of pure carbon-based nanostructures [2-7].

It is widely believed that in the future hydrogen will have a major role as an energy carrier, much more than it is today. Alcohols have proven to be particularly attractive and suitable for hydrogen production using low-temperature non-equilibrium plasmas [2, 8, 9], and they are used, for example in the development of Direct Alcohol Fuel Cells (PEMFC fuel cells) [10-12]. This sequence of technologies makes it possible to have production of fuel from the plants and thus achieve the most eco-friendly sustainable energy production and eventually consumption. Besides that, plasmas in alcohols are a good source of carbon and can be used for nanographene and nanotubes production [3-7]. A significant number of applications of these non-equilibrium discharges use sources of complicated electrode geometry. Those sources operate either in high current discharge regimes or in pulsed or high-frequency glow regime. Therefore, unravelling all processes taking place in the discharge is an exacting task.

A long-term interest for elementary collision and transport data in alcohol vapours originated from the development of elementary particle detectors [13-17]. The development of new applications demands the availability of a sufficient range and depth of data and of understanding of the phenomenology that are well tested by quantitative comparisons with experiments. These data can be obtained from studies of non-equilibrium discharges, either directly motivated by a very specific application or in quite generic experiments with a simple electrode geometry. Therefore, our measurements of Volt-Ampere characteristics in addition to the Paschen curves and emission profiles in non-equilibrium parallel-plate dc discharges in different alcohol vapours [18] aim at providing a comprehensive reference set of data that can be used in interpreting and modeling more complex discharges [16, 19-24]. Our investigation follows similar steps as our previous studies of discharges in water vapour and in argon [25, 26].

It has been shown previously [27-29] that Paschen curves provide only a limited understanding of the breakdown itself or in particular of the secondary electron yields [27, 29-32]. As it was predicted by phenomenological and physical theories as well as by simulations a three-dimensional breakdown mapping consisting of V_b, pd and jd^2 (where V_b is the breakdown voltage, p is the pressure and d is the gap in parallel plate geometry and j is the current density) is required for a complete description of the low-current discharge [26, 33]. Here, in figure 1 we show one example (for methanol) of such 3D mapping of V_b, pd and i characteristics. Note that the characteristics is presented as a function of the discharge current i, instead of jd^2, which is the proper scaling. The main point in figure 1 is that voltage-current characteristics is equally important in the analysis of the secondary electron yields as the Paschen curve.

Voltage--current characteristics (on their own or with support of other diagnostic techniques such as time resolved fast ICCD recording of the variation in the discharge profile, observations of the presence of oscillations and other) have been shown to be valuable source of information on the energy (i.e. E/N) dependence of the secondary electron yields [26, 29, 31, 34] on the presence of different modes of oscillations [31, 35] and on the transitions between different modes of operation of low and moderate current discharges. In particular, modelling of the low current, diffuse Townsend regime may be used to determine a wide range of atomic and molecular collision data and understand relative contributions of different processes. Thus, we extend our initial work on establishing breakdown voltages (i.e., Paschen curves) [18] by determining voltage-current characteristics to discern which dominant species partake in the breakdown and in initialization of the non-equilibrium plasma under those circumstances [36]. Preliminary results for ethanol vapour, along such line of research, have been published in [37]. In this paper, we extend our investigations to a wider range of conditions and to vapours of alcohols of different complexity.

The next step would be to apply all the theoretical/simulation tools, in similar fashion to what has been done for water vapour. Such modelling of well-defined experimental data may provide us with information on the most important processes and on the basic physical foundation of low temperature plasmas in water and alcohol vapours.

While there have been several published studies of, either breakdown voltage V_b versus pd (Paschen curves) or voltage-current characteristics of gas discharges, especially in the glow and dark Townsend regimes, we are not aware of any of such studies for alcohol vapours. With an improved theoretical understanding and a broader range of the available data this study is also well motivated by the need to produce a basis for a more comprehensive data set for pertinent processes and by the need to address possible applications (as listed here) by detailed modelling.

This paper is an attempt to extend the existing studies in alcohol vapours (see [24, 38-43]) with careful and well-defined procedure to measure the observables from the discharges in order to obtain some data on primary and secondary processes in a subsequent analysis.

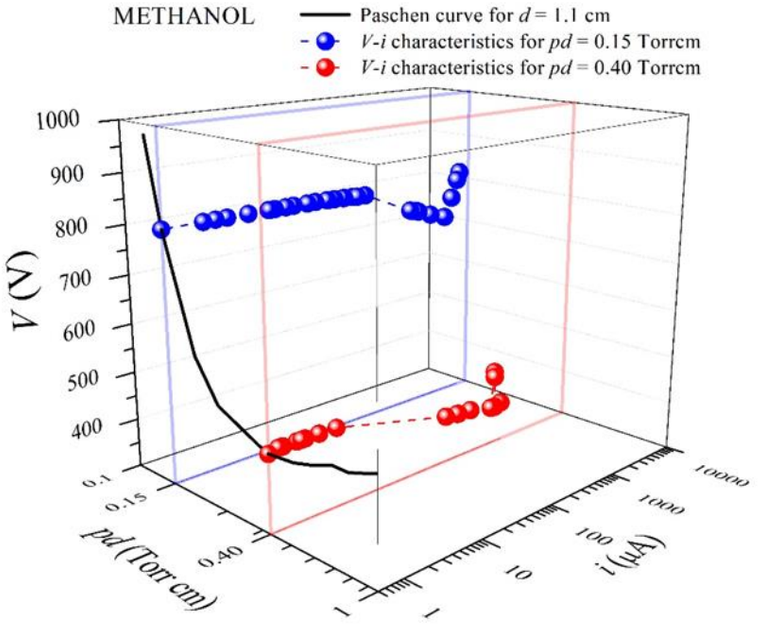

Figure 1. V_b, *pd* and *i* characteristics in methanol vapour discharge for electrode gape of 1.1 cm. The Paschen curve for discharge in methanol vapour have been presented in our earlier paper [18] while *V-i* characteristics for *pd*=0.15 and 0.40 Torr cm are shown in present paper in figure 3. The results presented here have been obtained by the experimental setup that will be described later in the present paper and has been described elsewhere as well [25, 36].

2 Experimental set- up

The schematic of the experimental setup (as described in previous papers [25, 36, 37, 44]) is shown in figure 2. The discharge chamber consists of parallel plane electrodes placed inside a tightly fitting quartz tube. Each of electrodes is 5.4 cm in diameter (*2r*). The cathode (C) is made of copper and the anode (A) is made of quartz covered by a thin, transparent, conductive platinum film. This arrangement allows us to observe radial profile of the discharge, constrictions, and diffuse regimes. The distance (*d*) between electrodes can be adjusted by fixed electrode supports and for this experiment it was set to 1.1 cm.

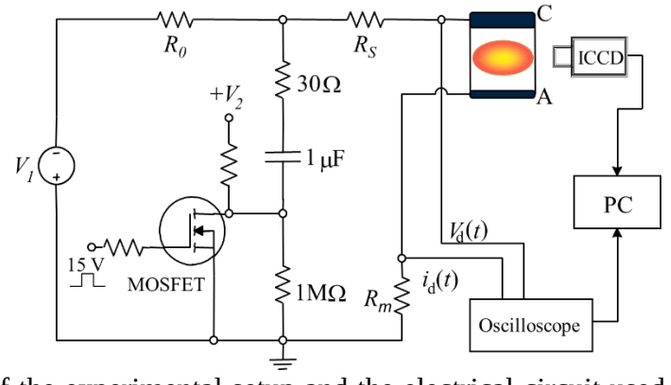

Figure 2. Schematic of the experimental setup and the electrical circuit used in measurements [25, 36].

To obtain reproducible results, it is necessary to perform preparations before every measurement. Initially, the system is pumped down to an initial pressure of the order of 10^{-6} Torr. Before the measurements, the cathode surface is conditioned in a hydrogen discharge with a current around 30 μA (for approximately 40 min), until operating voltage is stabilized. Hydrogen is chosen because it is lightweight, so no cathode material is dispersed and yet it has potential to remove oxide layers and react with organic vapours. At the same time, this treatment effectively removes chemical

oxides and adsorbed layers of impurities from the cathode surface and thus produces the same surface conditions for each measurement. After cleaning of the cathode, discharge chamber is again vacuumed to the pressure of around 10^{-6} Torr before flow of gas is introduced. Both, treatment in hydrogen discharge and measurements in alcohol vapours are done in a slow flow regime, to ensure that possible impurities formed in the discharge chamber are continuously removed and kept at low abundance. Most importantly our setup allows us to operate in a pulsed regime whereby current is maintained in a short period of time, sufficient to make measurement but too short so that damage to the cathode (due to sputtering) is avoided [26, 45, 46].

We have performed measurements for four alcohols: methanol, ethanol, isopropanol (2-propanol) and n-butanol. The vapours are obtained from 99.5% purity methanol, isopropanol, and n-butanol and 95% purity ethanol (see our earlier papers [18, 37]). For all the used alcohols in our measurements water represents the most abundant declared impurity (max. 0.2%), while other volatile impurities such as acetone, aldehydes, and formic acid (max. 0.002%) are present in smaller quantities. Also, only in traces, there is iron (0.0005%) and some non-volatile substances (<0.001%). Therefore, a small percentage of water vapour may be present in the discharge. The presence of inherent gas impurities can be critical in two cases: the existence of significant vibrational energy losses introduced by molecular impurities in rare gases (this can strongly affect the breakdown data in atomic gases as molecular impurities introduce significant energy losses below the threshold for electronic excitations) and in the occurrence of the attachment to impurities. However, neither of the two is expected to strongly affect the results for gas discharges where ionization is the key process and is dominated by the most abundant gas. Therefore, water will not affect the results strongly through either of the two mentioned mechanisms and the same is true for all other listed components.

The vapour is introduced into the chamber at low pressure from a container with a liquid sample, through a pressure regulatory valve at a low flow rate. Immediately after opening the valve alcohol begins to boil due to the pressure difference over above the surface and partial pressure of gases dissolved in the sample. Throughout this process alcohol becomes devoid of dissolved volatile constituents and after few seconds the sample surface becomes still. After that, the vapour is maintained at a moderate pressure, (lower than the vapor pressure) in the chamber for periods of 1–2 h to saturate the electrodes and the chamber walls. The vapour pressures of methanol, ethanol, isopropanol, and n-butanol at room temperature (25^{o}C), are around 127, 45, 44 and 7 Torr, respectively [47], so during the measurements operating pressures are kept well below these values to avoid formation of liquid droplets.

Our electrical circuit allows a current pulse of desired length and amplitude to be superimposed onto a dc discharge running at a very low current (typically around 1 μA), to avoid breakdown delays [26, 44]. Pulse duration is long enough so that a steady state discharge is developed and also sufficient to make reliable recordings. In this way, by minimizing gas heating and cathode heating and conditioning [44, 48], results of measurements of voltage-current characteristics (V-i) are stable and reproducible. Construction of the chamber allows recording of axial discharge profiles using a sensitive intensified ICCD (Andor IStar DH720-18U-03). For spectrally resolved measurements of spatial distribution of emission intensity, we used a bandpass optical filter in front of the lens which enabled recordings of emission profiles for a CH band at 431.2 nm.

3 Results and discussion

3.1 Voltage-current characteristics

In figure 3 we show voltage-current characteristics of low to moderate current discharges in four alcohol vapours: methanol, ethanol, isopropanol, and n-butanol recorded at electrode distances of 1.1 cm for two pd values. The results obtained for different combinations of resistors R_s and R_m are represented by different symbols. The voltage is represented at y-axis by ΔV, as the difference between the discharge voltage V and the breakdown voltage V_b. This way of the result presentation

eliminates small differences in breakdown voltages in different sets of measured data, which do not affect the 'dynamic' voltage-current characteristics [48, 49]. At the same time presenting the difference in voltage before and after the breakdown makes it possible to show small changes in the voltage that would be otherwise too small to observe on top of a large breakdown voltage.

The recorded voltage-current characteristics clearly show the areas of different operating modes through which the discharge passes with increasing of the current: Townsend discharge (low-current discharge), normal glow discharge and abnormal glow discharge (in fig.3 the operating regimes are marked in graphs with letters a-c, respectively) [36]. The break in the voltage-current characteristics matches the area of free running, undamped oscillations. This area expands with an increase in the gas pressure. It can be seen that the abnormal discharge regime has a higher slope at higher pressures, for all alcohol vapours presented here. This is in contrast with the water vapor where higher slopes have been recorded at lower pressures [25].

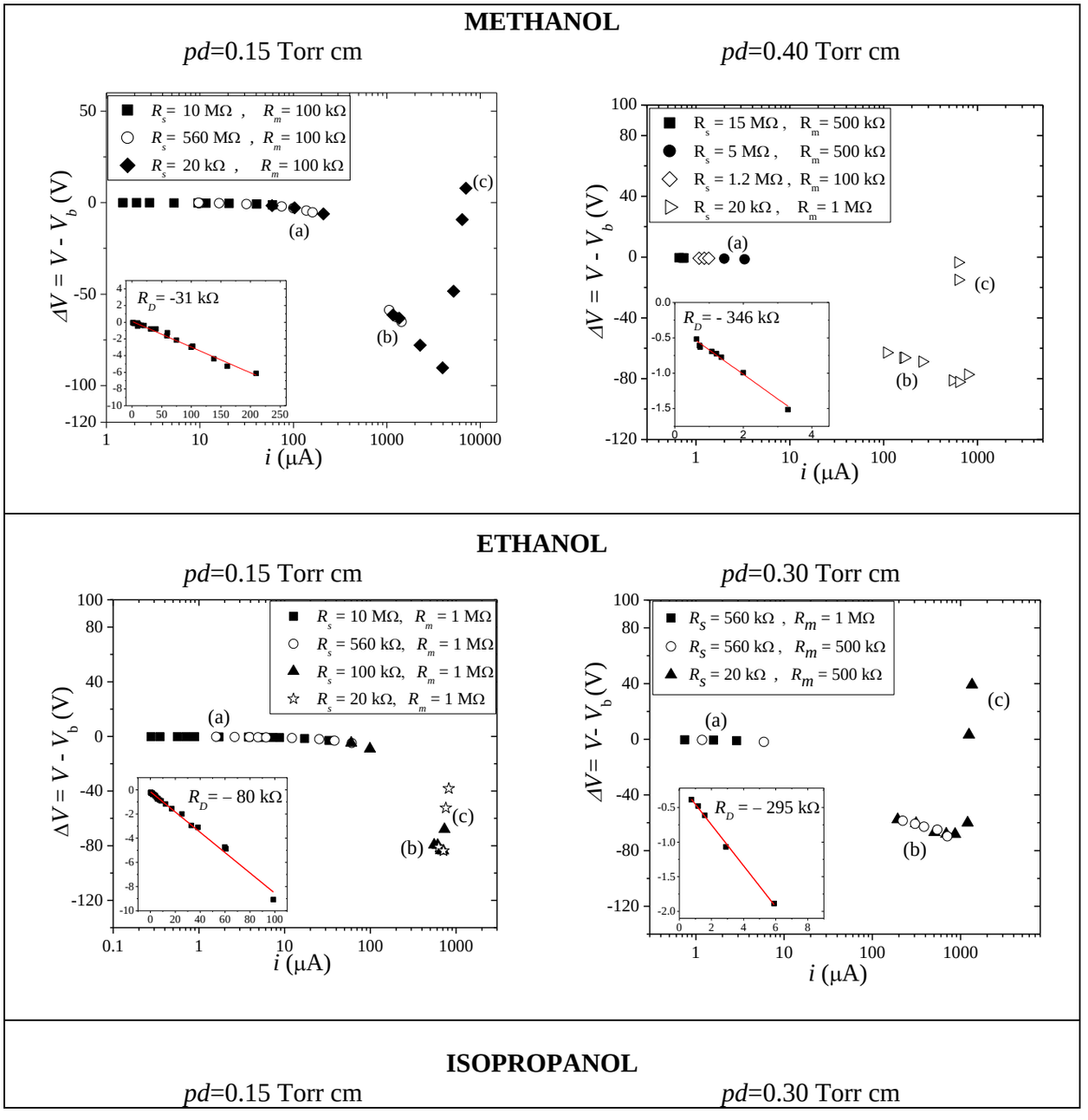

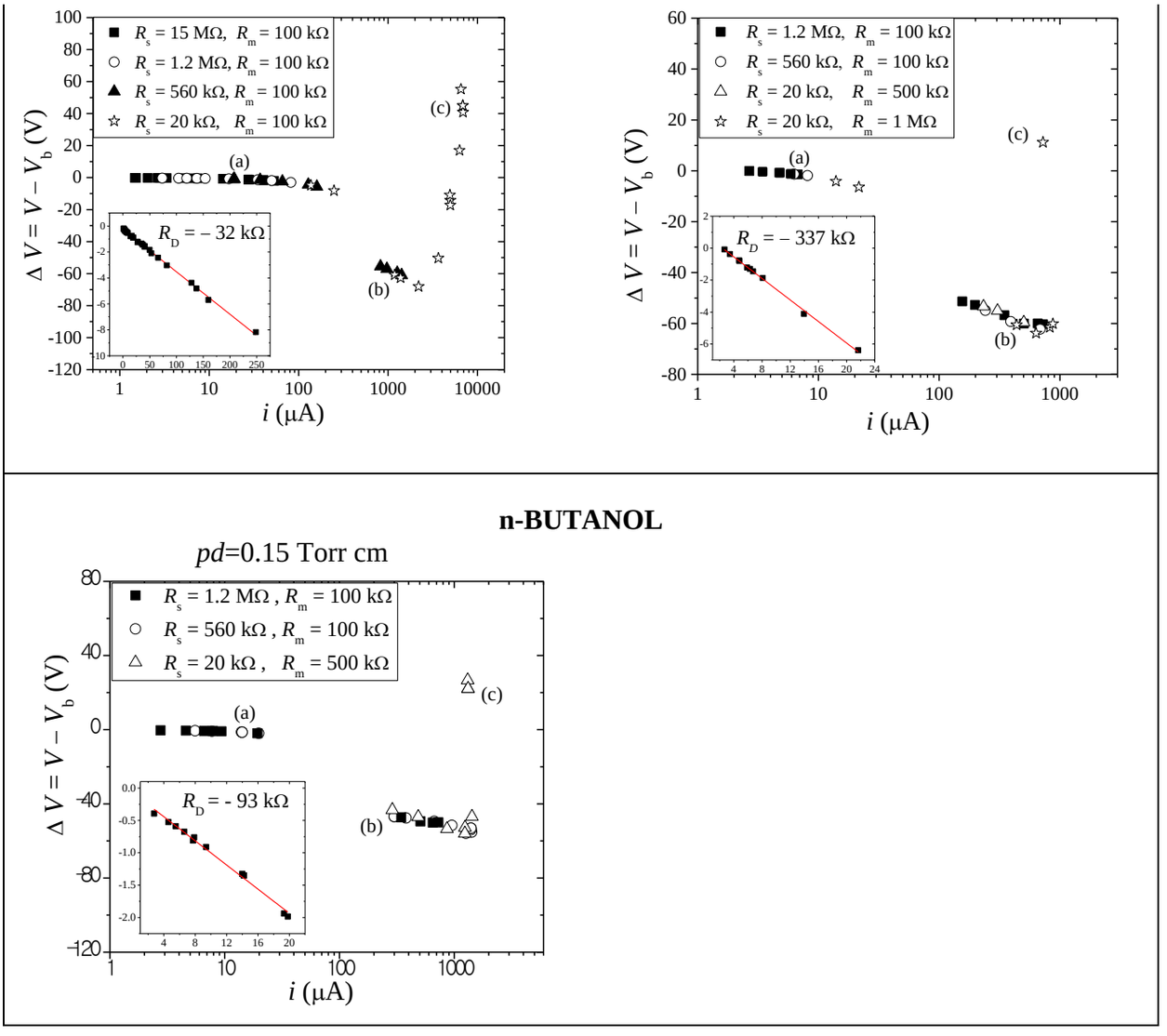

Figure 3. Voltage-current characteristics for low-pressure dc discharges in alcohol vapours recorded at d=1.1 cm at different pd values: in the left-hand branch of Paschen curve – pd = 0.15 Torr cm and at the minimum of the Paschen curves – pd = 0.40 and 0.30 Torr cm. V is discharge voltage, while V_b denotes the breakdown voltage. Inserted graphs show negative differential resistance R_D that are obtained in our experiment for the steady state Townsend regime.

The negative differential resistance R_D at the lowest currents is determined for the steady state (or dark) Townsend regime and it has been determined by fitting the low-current portion of the measured voltage-current characteristics (the fits and the results are presented in inserted graphs in fig. 3). In other words, the negative slope of the Townsend discharge area (in fig.3 marked with the letter (a) on the graphs) corresponds to negative differential resistance. Negative differential resistance is a consequence of the spatial charge effects that occur due to the increase of the discharge current [31, 45], as well as the dependence of the secondary electron emission on the current and discharge voltage. A positive spatial charge effectively increases the electric field in front of the cathode, thereby exponentially increasing the ionization coefficient and the secondary electron yield, allowing the stable operation of the discharge at a lower voltage. Thus, an increase in the concentration of the spatial charge leads to inhomogeneity of the field, which in turn causes a decrease in the discharge voltage.

Simultaneously with measurements of voltage and current i.e., V-i characteristics we recorded corresponding spatial distributions of light emission from discharge, that were used to obtaining

axial profiles of emission (fig.4). At this point we try to illustrate different regimes. A more thorough representation of spatial profiles will be presented when we develop a complete modelling set that would provide contributions of different high energy particles to emission and consequently their role in the breakdown. These recordings include spatial profiles of the total emission in a visual spectral range and spatial distribution of emission in a narrow wavelength interval around the most intense lines in the visible part of the spectrum (for CH band at 431.2 nm).

In figure 4 we show examples of spatial emission profiles at two *pd* values (0.15 and 0.40 Torr cm) in methanol vapour discharge that indicate how emission profiles may be used for identification of the discharge operation regime, and from additional information and modelling one may identify the pertinent physical agents that contribute to the discharge under those conditions.

From the axial emission profiles obtained for *pd*=0.15 Torr cm (fig. 4(I)) in methanol vapour discharge in all regimes, processes induced by heavy particles play a major role in excitation and ionization of gas/vapour, which is revealed in the existence of the peak of intensity in front of the cathode [50, 51]. Also, CH profile (dashed line) follows the shape of the total profile (solid line), With increasing current, the contribution of electron processes increase in discharge – the noticeable higher peak of intensity in front of the anode (fig. 4(Ib) and 4(Ic)). In all regimes, the CH profile (dashed line) has a maximum peak in front of the cathode.

At higher pressure, at *pd* that corresponds to the minimum of the Paschen curve for methanol vapour discharge (*pd*=0.40 Torr cm, fig. 4(II)) the processes induced by heavy particles and electrons have almost equal contributions in excitation – maximum intensities of emission in front electrodes are approximately equal (solid line) (fig. 4(IIa)).

Electrons are accelerated towards the anode and they multiply followed by exponentially rising emission profile as the equilibration of electrons is rather fast. The ions produced in ionizations move towards the cathode gaining energy. The growth of ion density and related emission profile are not exponential but the density peaks by the cathode. It has been assumed in the past that these ions produce excitation in collisions with gas molecules, but due to the shape of their cross-sections, ions begin to contribute only at very high energies [51-55]. At energies characteristics of the ions in standard Townsend discharges the excitation peaking towards the cathode was shown to be due to fast neutrals produced from the fast ions in charge exchange collisions. Such collisions leave ions standing still while neutrals leave the collision with close to the full energy of the projectile ion. Fast neutrals may also reflect from the cathode and move towards the anode, thus giving two distinct wings to the emission line profiles.

Presented axial emission profiles, for both *pd* values, show that with the increase of current, the intensity of emission also increases and reaches its maximum in abnormal glow regime. Furthermore, the peak of emission in front of the anode (fig. 4(Ic) and 4(IIc)) shifts towards the cathode with increasing current, which is a consequence of the formation and development of the cathode fall. Namely, the position of the peak of emission intensity in front of the anode corresponds to the maximum of negative glow, which coincides with the edge of the cathode fall [44]. As the length of the cathode fall almost coincides with the distance between the electrodes at low pressures, these changes are not very pronounced (fig. 4(Ib) and 4(Ic)).

At the higher pressures (0.40 Torr cm) after passing through the oscillation mode, the discharge enters the normal glow mode in a visibly constricted mode (fig. 4(IIb)). In the constricted mode, the radial spatial distribution of the discharge is narrowed and occupies only a part of the surface on the electrode (fig. 4(IIb)). The very appearance of the constricted discharge mode is conditioned by the existence of an extremely rapid increase in the ionization coefficient with the increasing of the electric field [36]. The constriction is not very pronounced in the interval of high values of the reduced electric field *E/N* i.e., lower *pd*=0.15 Torr cm, due to a slight increase in the ionization

coefficient at the transition from low-current diffuse to a normal glow discharge and longer diffusion length at lower pressure.

I) *pd* = 0.15 Torr cm

(a) i = 138 μA

TOWNSEND DISCHARGE

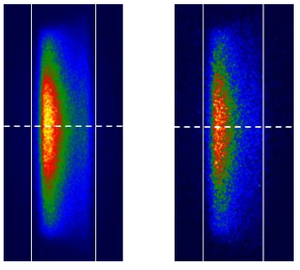

total emission CH filter

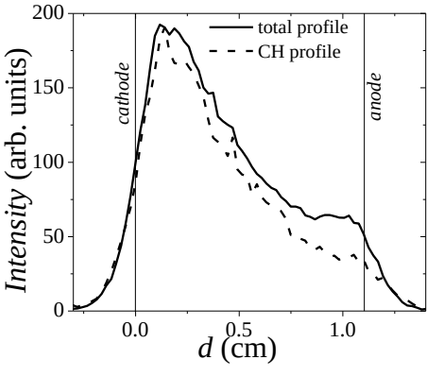

(b) i = 1665 μA

NORMAL GLOW DISCHARGE

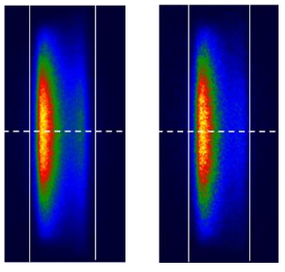

total emission CH filter

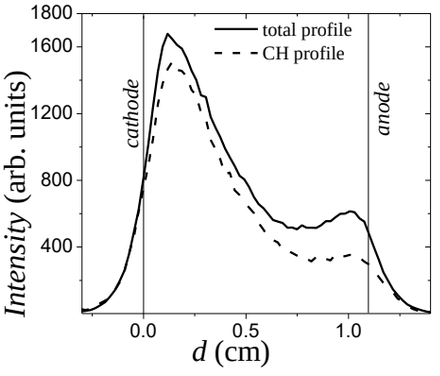

(c) i =7013 μA

ABNORMAL GLOW DISCHARGE

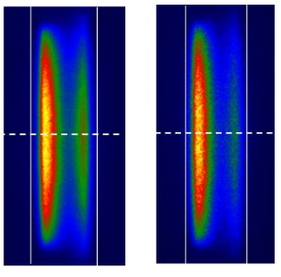

total emisssion CH filter

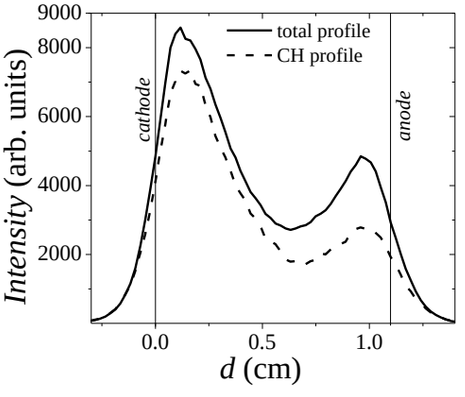

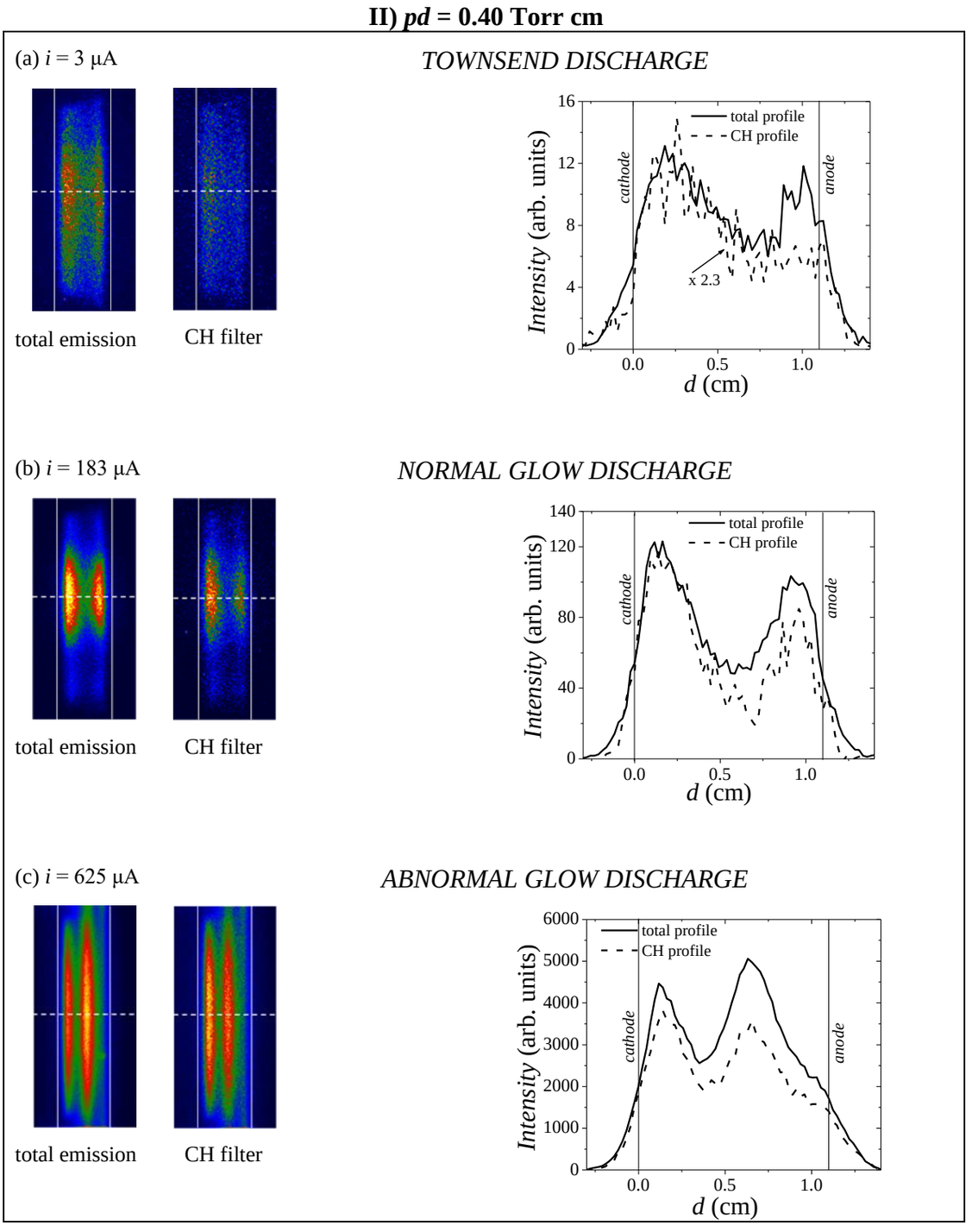

Figure 4. Axial profiles of emission for discharges in methanol vapour discharge for I) *pd*=0.15 Torr cm and II) 0.40 Torr cm, obtained along with the recording of voltage-current characteristics at *d*=1.1 cm that correspond to different regimes marked on the graph with letters a-c in fig.3. CH profile of Townsend emission at *pd* = 0.40 Torr cm was multiplied with a factor of 2.3 for easier comparison with a profile of total emission in the visible spectrum.

3.2 Mode transition

During our investigation of abnormal glow in methanol vapour, as a part of the study of the voltage-current characteristics, we observed sudden changes in the operating conditions at *pd*=0.40 Torr cm (fig.5). These changes in operation mode were previously observed in ethanol vapour discharge as

shown in our previous article [37]. Measurements in methanol vapour at higher currents reveal changes in the steady-state current and voltage values within a single voltage pulse. The discharge operates at a lower current and higher voltage after the transition.

We performed time-resolved measurements at higher currents in abnormal regime to better perceive and understand what is happening in discharge when this mode transition is occurring. The time-resolved measurements were done for points that are marked in figure 5 by open circles. At the same graph full circles represent the voltage and current values before the discharge mode transition (before the step) that match the values marked at figure 6.

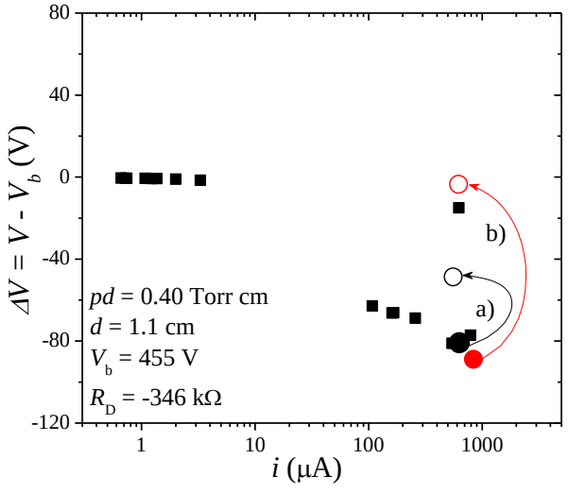

Figure 5. Voltage-current characteristics for methanol vapour discharge at *pd*=0.40 Torr cm and *d*=1.1 cm. Voltage ΔV represent difference between discharge voltage (V) and breakdown voltage (V_b = 455 V). The discharge mode shift is denoted by arrows and symbols (circles) that correspond to values from fig. 6.

Figure 6 shows examples of step-like transitions in voltage and current waveforms that occur at two different initial currents: a) 630 μA and b) 840 μA. In first case that is shown in fig.6a) the mode transition is happening approximately 0.2 ms after the pulse ignition. During the transition discharge switches to ~30 V higher voltage and ~ 70 μA lower current. The transition is smooth and lasts around 4 μs. In case of higher initial current (fig.6b) the transition occurs ~2 ms after the beginning of the pulse and after the transition (the 'step'), discharge operates at ~70 V higher voltage and ~200 μA lower current. The transition lasts approximately ~ 10 μs. It is important to emphasize that in both cases the transition from one discharge mode to another is smooth, without any observable instabilities or oscillations in voltage and current signals.

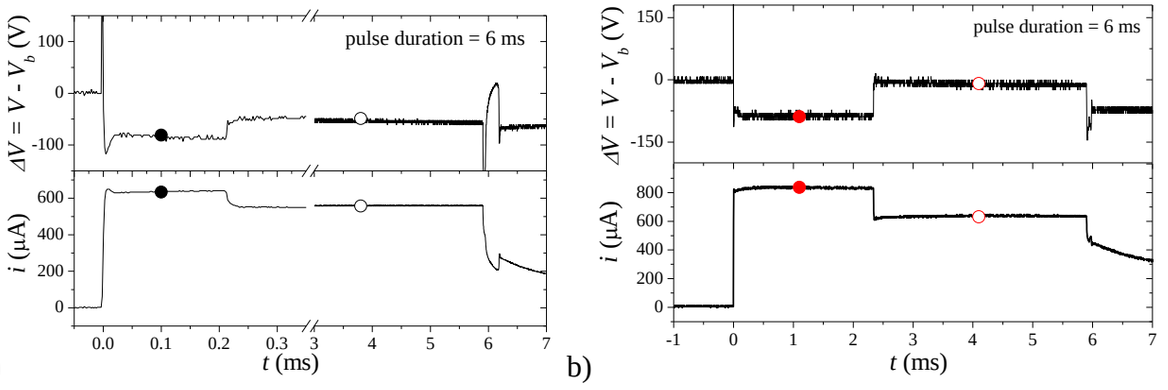

Figure 6. Voltage and current waveforms obtained in methanol vapour discharge at a) lower initial current i = 630 μA and b) higher initial current i = 840 μA, with step-like transitions that ocurrs

during one pulse. Voltage ΔV represents the difference between discharge voltage (V) and breakdown voltage (V_b = 455 V). Voltage and current values before (full symbols) and after (open symbols) the step transition correspond to values from fig.5.

Together with voltage and current measurements we recorded 2D images of light emission from the discharge at several moments before and after the step-like transition within a single pulse (figure 7). These images provide axial profiles of emission of the discharge (figure 8) by extracting the intensity vector along the longitudinal axis of the discharge chamber. Thus we may discern the changes in the mode of operation. We also used optical filter for CH band at 431.2 nm that enabled comparison with total axial profiles of emission obtained by integrating the whole visual spectrum (2D images in fig.7a).

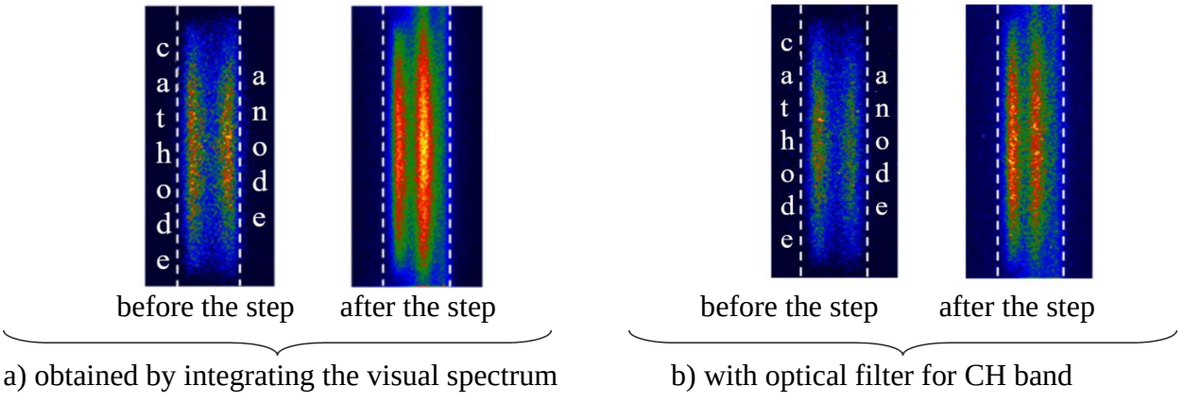

Figure 7. 2D images of discharge, obtained along the chamber longitudinal axis, that corresponds to moments before and after the step-like transition (in fig. 6b)): a) images obtained by integrating the visual spectrum and b) images obtained using an optical filter to extract the wavelength corresponding to the CH band at 431.2 nm.

Figure 8 shows a) total and b) CH axial profiles of emission before and after the 'step' transition. In both cases, profiles before and after the 'step' have a peak close to the cathode indicating that excitation by heavy particles [26, 50] is significant. Also, after the transition the overall intensity of emission is higher, even though the discharge current drops. The ratio of the contribution of heavy particles and electrons to the emission intensity remains the same.

Moreover, from the radial profiles of emission (fig.9) obtained from the 2D images of the discharge taken before and after the 'step' transition (fig.7) it can be seen that both profiles have the same width and therefore the same effective discharge area [33]. That means that the normal glow has reached its maximum width and is about to make transition to the abnormal glow.

The main difference in the profiles before and after the step is the position of emission peak that corresponds to the negative glow i.e. coincides with the edge of the cathode fall d_{CF} [44]. The edge of the cathode fall region shifts closer to the cathode after the transition, which seems to be in contradiction to the decrease of discharge current, but is consistent with an increase in E/N. In any case, we may conclude that the transition shown here represents a direct observation of the transition from a normal to the abnormal glow discharge mode. The fact that the current decreases in transition to the abnormal glow means that the space charge is formed and with sufficient increase in the local E/N (higher voltage and shorter cathode fall) it compensates for the losses in excitation and ionization due to somewhat decreased current. It is not linear extrapolation as here we deal with sheaths of different voltage and length.

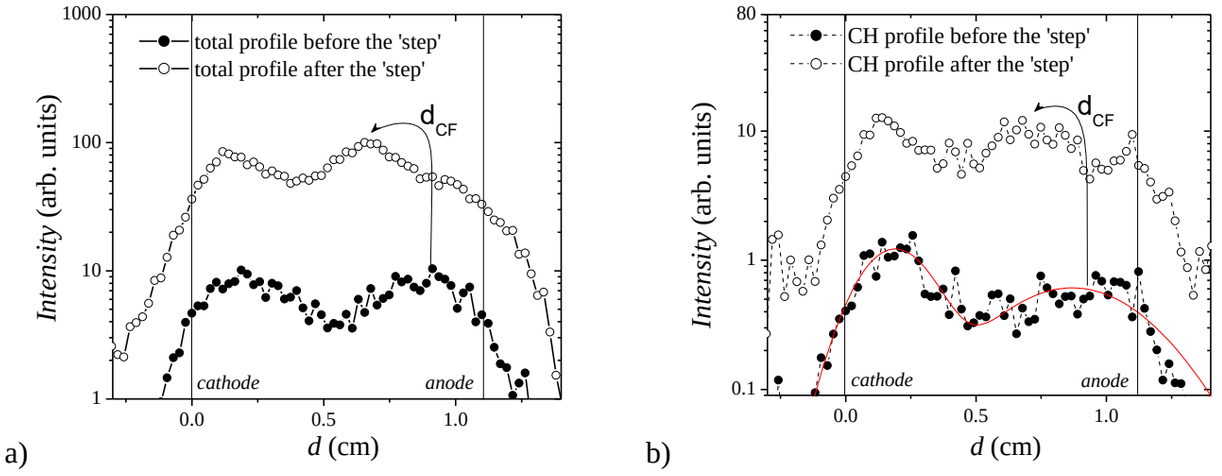

Figure 8. Axial profiles of emission for methanol vapor obtained from 2D images (figure 7) at moments before (full symbols) and after (open symbols) the step-like transitions that corresponding to the points given in Figure 6b). Here we give a comparison of: a) the total emission profiles before (full symbols) and after (open symbols) and b) the CH band emission profiles before (full symbols) and after (open symbols) the mode transition. The CH profile before the step is fitted with a function that is the sum of two Gaussians (red line) for easier identification of the maximum intensity in front of the anode. The changes in the initial values of voltage and current in the steady-state after the step transition are $\delta V = 70$ V, $\delta i = -200$ μA. The length of cathode fall is denoted by d_{CF}.

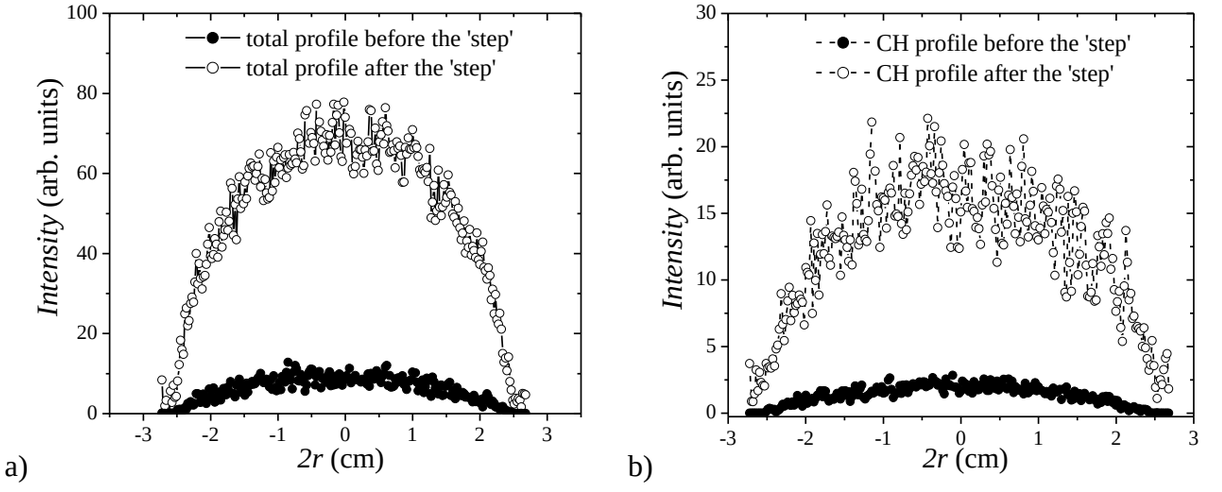

Figure 9. Radial profiles of emission in methanol vapour discharge: a) total radial profiles and b) CH radial profiles, in moments before (full symbols) and after (open symbols) the step-like transition that corresponds to points given at fig. 6b.

4 Conclusion

In this paper we have provided experimental recordings of the voltage-current (*V-i*) characteristics of discharges in four different, yet common, alcohols covering Townsends, normal glow, and abnormal glow regimes (low current diffuse, constricted, and high current diffuse in Phelps' terminology). Such data for alcohols have not been hitherto available.

The Townsend regime characteristics apart from values of breakdown voltage provide the negative differential resistance as a quantitative measure of the space charge effects [51]. We may notice a strong dependence of R_D with *pd*. Spatial emission profiles in this regime may also be fitted by theoretical/numerical results and used to obtain data on elementary atomic and molecular collision

processes such as ionization rates and cross-sections, total excitation/dissociation rates induced both by electrons and by heavy particles in particular fast neutrals [50]. All these data are lacking for the alcohols (both as vapours and liquids as the background for discharges leading to the production of a non-equilibrium plasma). Present results for spatial emission profiles, if normalized to absolute values, may be the basis to produce quantitative data. Such normalization is possible as we maintained relative calibration of the sensitivity. Here we present results for the overall emission (that, as expected, has the best statistics) and for the CH band emission that is the strongest component of the total emission. Both show significant heavy particle excitation increasing with the *E/N*. Nevertheless, we have found an emission band that is not excited by the heavy particles in the region of mean energies and operating fields covered here.

Following the progression of the *V-i* characteristics to the region of the normal glow (through the unstable domain of the Townsend to normal glow transition) one can see the correspondence between the spatial profiles of the discharges in different modes and the *V-i* characteristics. The difference in voltage between the normal glow and the breakdown voltage is an important factor as well as the slope of the load line for the stability of operation of the discharge.

Finally, we have observed a distinct transition between a normal and an abnormal glow regime occurring within a limited time and leading to observable rearrangement of the field and plasma profile, also leading to much more efficient production of photons (and presumably ionization). The mode transition so far has been observed for argon [56], and for ethanol too [37]. In this case, we have provided the most systematic measurement, as a basis for possible modelling of those data. It may also be used to test and verify plasma modelling codes in the domain of representing space charge effects [57, 58]. The 'step' in the voltage indicates the transition between two regimes of operation that may not be in stable equilibrium, to begin with. The transition is clearly between the normal and the abnormal glow regimes and may be induced by a number of processes (heating of the gas, conditioning of the cathode, external perturbation, gradual slow growth of the space charge…). It may also be associated with different radial profiles of the discharge. Such transitions are more easily observed when discharge oscillates with different regimes of oscillations in the pre- and post-transition domains. This is not the case here. Interestingly in the present case, for both methanol and ethanol, radial profiles in the two regimes are not observably different. In any case, gases where such transitions were observed, for a very narrow range of conditions, are very few.

The elementary processes in alcohol vapours and liquids may lead to a wealth of products and may initiate further chemical reaction chains that may be used for a number of purposes. Of the more direct applications, one may benefit from the extended knowledge of the breakdown in alcohol vapours having in mind applications such as using alcohols as combustion fuels, nano-structure growth in discharges through liquids and in using admixtures of different molecules in atmospheric pressure plasmas for various biotechnical procedures. On a separate plane, one should mention the development of the elementary particle detectors, the new generations where optimized design may improve performance significantly.

Acknowledgments

The authors acknowledge support from the Serbian Ministry of Education, Science and Technological Development under project numbers OI 171037 and III 41011. One of the authors (ZLP) is grateful to the SASA project 155 and to the Ulster University for partial support.

Data availability

The data that support the findings of this study are available from the corresponding authors upon reasonable request.

References

1. P. J. Bruggeman, M. Kushner, B. Locke, H. Gardeniers, B. Graham, D. Graves, R. Hofman-Caris, D. Marić, J. Reid, E. Ceriani, D. Fernandez Rivas, J. Foster, S. Garrick, Y. Gorbanev, S. Hamaguchi, F. Iza, H. Jablonowski, E. Klimova, F. Krcma, J. Kolb, P. Lukes, Z. Machala, I. Marinov, D. Mariotti, S. Mededovic Thagard, D. Minakata, E. Neyts, J. Pawlat, Z. Lj. Petrović, R. Pflieger, S. Reuter, D. Schram, S. Schroeter, M. Shiraiwa, B. Tarabova, P. Tsai, J. Verlet, T. von Woedtke, K. Wilson, K. Yasui, G. Zvereva, Plasma Sources Sci. Technol. **25**, 053002 (2016)

2. G. Petitpas, J. D. Rollier, A. Darmonb, J. Gonzalez-Aguilar, R. Metkemeijer and L. Fulcheri, Int. J. Hydrogen Energy **32**, 2848 (2007)

3. S. Maruyama, R. Kojimaa, Y. Miyauchia, S. Chiashia and M. Kohnob, Chem. Phys. Lett. **360**, 229 (2002)

4. M. Matsushima, M. Noda, T. Yoshida, H. Kato, G. Kalita, T. Kizuki, H. Uchida, M. Umeno and K. Wakita, J. Appl. Phys. **113**, 114304 (2013)

5. A. Ando, K. Ishikawa, H. Kondo, T. Tsutsumi, K. Takeda, T. Ohta, M. Ito, M. Hiramatsu, M. Sekine and M. Hori, Japanese Journal of Applied Physics **57**, 026201 (2018)

6. A. Kumar, P. A. Lin, A. Xue, B. Hao, Y. K. Yap and R. M. Sankaran, Nat. Commun. **4**, 2618 (2013)

7. N. Tarasenka, A. Stupak, N. Tarasenko, S. Chakrabarti, and D. Mariotti, Chem. Phys. Chem. **18**, 1074 (2017)

8. M. G. Sobacchi, A. V. Saveliev, A. A. Fridman, L. A. Kennedy, S. Ahmed and T. Krause, International Journal of Hydrogen Energy **27**, 635 (2002)

9. F. Chen, X. Huang, D. Cheng and X. Zhan, International Journal of Hydrogen Energy, **39**, 9036 (2014)

10. R. Dillon, S. Srinivasan, A. S. Aricò and V. Antonucci, J. Power Sources **127**, 112 (2004)

11. M. Z. F. Kamarudin, S. K. Kamarudin, M. S. Masdar and W. R. W. Daud, International journal of hydrogen energy **38**, 9438 (2013)

12. R-C. Zhang, D. Sun, R. Zhang, W-F. Lin, M. Macias-Montero, J. Patel, S. Askari, C. McDonald, D. Mariotti and P. Maguire, Scientific Reports **7**, 46682 (2017)|

13. D. J. Grey, R. K. Sood and R. K. Manchanda, Nucl. Instr. Meth. A **527**, 493 (2004)

14. D. Bošnjaković, Z. Lj. Petrović, R. D. White and S. Dujko, J. Phys. D: Appl. Phys. **47**, 435203 (2014)

15. J. Va'vra, Nuclear Instruments and Methods in Physics Research A **515**, 1 (2003)

16. M. G. Curtis and I. C. Walker, J. Chem. Soc., Faraday Trans. **88**, 2805 (1992)

17. T. L. Cottrell and I. C. Walker, Trans. Faraday Soc. **61**, 1585 (1965)

18. J. Sivoš, D. Marić, G. Malović and Z. Lj. Petrović, Eur. Phys. J. D **74**, 64 (2020)

19. I. Adamovich, S. D. Baalrud, A. Bogaerts, P. J. Bruggeman, M. Cappelli, V. Colombo, U. Czarnetzki, U. Ebert, J. G. Eden, P. Favia, D. B. Graves, S. Hamaguchi, G. Hieftje, M. Hori, I. D. Kaganovich, U. Kortshagen, M. J. Kushner, N. J. Mason, S. Mazouffre, S. Mededovic Thagard, H-R. Metelmann, A. Mizuno, E. Moreau, A. B. Murphy, B. A. Niemira, G. S. Oehrlein, Z. Lj. Petrovic, L. C. Pitchford, Y-K. Pu, S. Rauf, O. Sakai, S. Samukawa, S. Starikovskaia, J. Tennyson, K. Terashima, M. M. Turner, M. C. M. van de Sanden and A. Vardelle, J. Phys. D: Appl. Phys. **50**, 323001 (2017)

20. J. Tennyson, S. Rahimi, C. Hill, L. Tse, A. Vibhakar, D. Akello-Egwel1, D. B. Brown, A. Dzarasova, J. R. Hamilton, D. Jaksch, S. Mohr, K. Wren-Little, J. Bruckmeier, A. Agarwal, K. Bartschat, A. Bogaerts, J. P. Booth, M. J. Goeckner, K. Hassouni, Y. Itikawa, B. J. Braams, E. Krishnakumar, A. Laricchiuta, N. J. Mason, S. Pandey, Z. Lj. Petrovic, Yi-Kang Pu, A. Ranjan, S. Rauf, J. Schulze, M. M. Turner, P. Ventzek, J. C. Whitehead and Jung-Sik Yoon, Plasma Sources Sci. Technol. **26**, 055014 (2017)

21. S. Ghosh, K. L. Nixon, W. A. D. Pires, R. A. A. Amorim, R. F. C. Neves, H. V. Duque, D. G. M. da Silva, D. B. Jones, F. Blanco, G. Garcia, M. J. Brunger, M. C. A. Lopes, International Journal of Mass Spectrometry, **430**, 44 (2018)

22. X-D. Wang, C-J. Xuan, W-L. Feng, and S. X. Tian, The Journal of Chemical Physics **142**, 064316 (2015)

23. D. G. M. da Silva, M. Gomes, S. Ghosh, I. F. L. Silva, W. A. D. Pires, D. B. Jones, F. Blanco, G. Garcia, S. J. Buckman, M. J. Brunger and M. C. A. Lopes, The Journal of Chemical Physics **147**, 194307 (2017)

24. M. J. Brunger, International Reviews in Physical Chemistry **36**, 333 (2017)

25. J. Sivoš, N. Škoro, D. Marić, G. Malović and Z. Lj. Petrović, J. Phys. D: Appl. Phys. **48**, 424011 (2015)

26. D. Marić, P. Hartmann, G. Malović, Z. Donkó and Z. Lj. Petrović, J. Phys. D: Appl. Phys. **36**, 2639 (2003)

27. D. Marić, M. Savić, J. Sivoš, N. Škoro, M. Radmilović-Radjenović, G. Malović and Z. Lj. Petrović, Eur. Phys. J. D **68**, 155 (2014)

28. A. V. Phelps and Z. Lj. Petrović, Plasma Sources Sci. Technol. **8**, R21 (1999)

29. M. M. Nikolić, A. R. Đorđević, I. Stefanović, S. Vrhovac and Z. Lj. Petrovic, IEEE Trans. Plasma Sci. **31**, 717 (2003)

30. A. V. Phelps, L. C. Pitchford, C. Pedoussat and Z. Donko, Plasma Sources Sci. Technol. **8**, B1 (1999)

31. A. V. Phelps, Z. Lj. Petrović and B. M. Jelenković, Phys. Rev. E **47**, 2825 (1993)

32. M. S. Mokrov and Yu P. Raizer, Plasma Sources Sci. Technol. **17**, 035031 (2008)

33. N. Škoro, D. Marić and Z. Lj. Petrović, IEEE Trans. Plasma Sci. **36**, 994 (2008)

34. P. Hartmann, Z. Donkó, G. Bánó, L. Szalai and K. Rózsa, Plasma Sources Sci. Technol. **9**, 183 (2000)

35. Z. Lj. Petrović, I. Stefanović, S. Vrhovac and J. Živković, J. Phys. IV France **7**, C4-341 (1997)

36. D. Marić, G. Malović and Z. Lj. Petrović, Plasma Sources Sci. Technol. **18**, 034009 (2009)

37. J. Sivoš, D. Marić, N. Škoro, G. Malović and Z. Lj. Petrović, Plasma Sources Sci. Technol. **28**, 055011 (2019)

38. H. Hasegawa and H. Date, Journal of Applied Physics **117**, 133302 (2015)

39. R. Rejoub, C. D. Morton, B. G. Lindsay, and R. F. Stebbings, J. Chem. Phys. **118**, 1756 (2003)

40. C. Ni, D. Carolan, C. Rocks, J. Hui, Z. Fang, D. B. Padmanaban, J. Ni, D. Xie, P. Maguire, J. T.S. Irvine and D. Mariotti, Green Chem. **20**, 2101 (2018)

41. A. A. General, A. K. Shuaibov, V. A. Kel'man, Yu. V. Zhmenyak, Tech. Phys. Lett. **40**, 482 (2014)

42. A. I. Shchedrin, D. S. Levko, V. Ya. Chernyak, V. V. Yukhimenko and V. V. Naumov, Technical Physics Letters volume **35**, 449 (2009)

43. J. R. Ferrell, E. R. Bogovich, N. R. Lee, R. L. Gray, and D. D. Pappas, Biointerphases **10**, 021001 (2015)

44. D. Marić, K. Kutasi, G. Malović, Z. Donkó and Z. Lj. Petrović, Eur. Phys. J. D **21**, 73 (2002)

45. S. Živanov, J. Živković, I. Stefanović, S. Vrhovac and Z. Lj. Petrović, Eur. Phys. J. Appl. Phys. **11,** 59 (2000)

46. I. Stefanović and Z. Lj. Petrović, Japan. J. Appl. Phys. **36**, 4728 (1997)

47. R. C. Weast, in *Handbook of Chemistry and Physics*, 51st edn. (Ohio: Chemical Rubber Co, Cleveland, Ohio: 1970)

48. Z. Lj. Petrović and A. V. Phelps, Phys. Rev. E **47**, 2806 (1993)

49. B. M. Jelenković, K. Rózsa and A. V. Phelps, Phys. Rev. E **47**, 2816 (1993)

50. Z. Lj. Petrović and A. V. Phelps, Phys. Rev. E **80**, 016408 (2009)

51. Z. Lj. Petrović, B. M. Jelenković and A. V. Phelps, Phys. Rev. Lett. **68**, 325 (1992)

52. A. V. Phelps and B. M. Jelenković, Phis. Rev. A **38**, 2975 (1988)

53. Z. Lj. Petrović and A. V. Phelps, Physical Review E **80**, 066401 (2009)

54. V. Stojanović, Ž. Nikitović, Z. Lj, Petrović, IEEE Trans. Plasma Sci. **39**, 2592 (2011)

55. Z. Lj. Petrović and V. D. Stojanović, J. Vac. Sci. Technol. A **16**, 329 (1998)

56. Z. Lj. Petrović and A. V Phelps, Phys. Rev. E **56**, 5920 (1997)

57. A. Fierro, E. Barnat, M. Hopkins, C. Moore, G. Radtke, B. Yee, European Physical Journal D (2021) (accepted manuscript)

58. M. Turner, Plasma Sources Science and Technology **25**, 054007 (2016)

Journal of Applied Physics

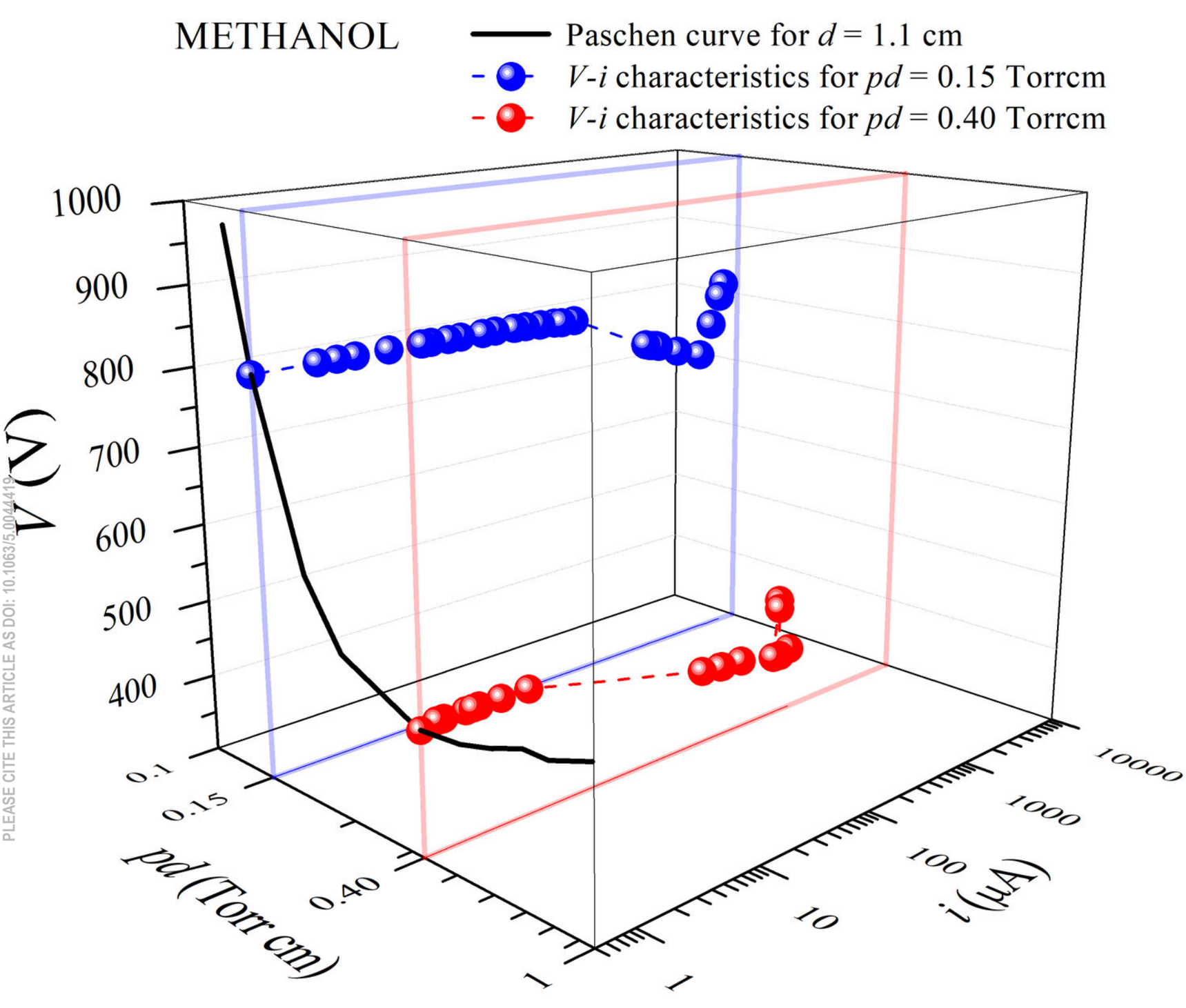

AIP Publishing

AIP Publishing

Journal of Applied Physics

ACCEPTED MANUSCRIPT

This is the author's peer reviewed, accepted manuscript. However, the online version of record will be different from this version once it has been copyedited and typeset.
PLEASE CITE THIS ARTICLE AS DOI: 10.1063/5.0044419

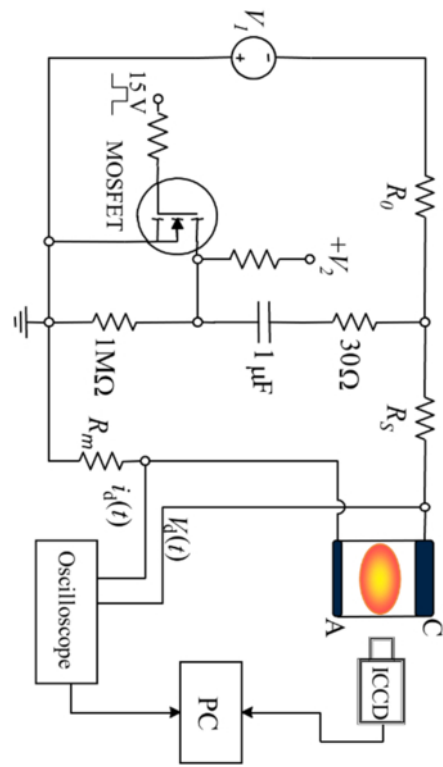

Journal of Applied Physics

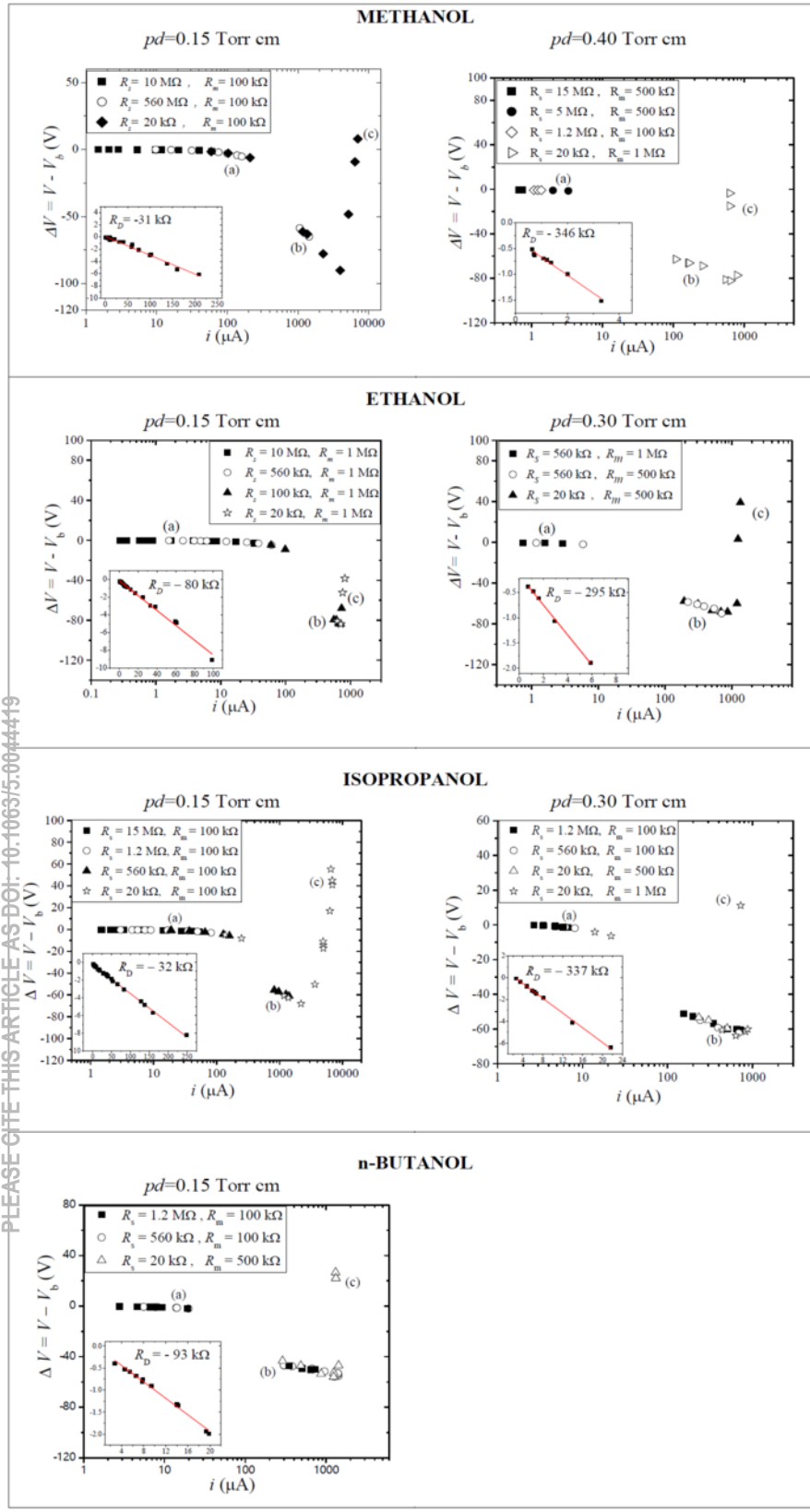

Journal of Applied Physics

AIP Publishing

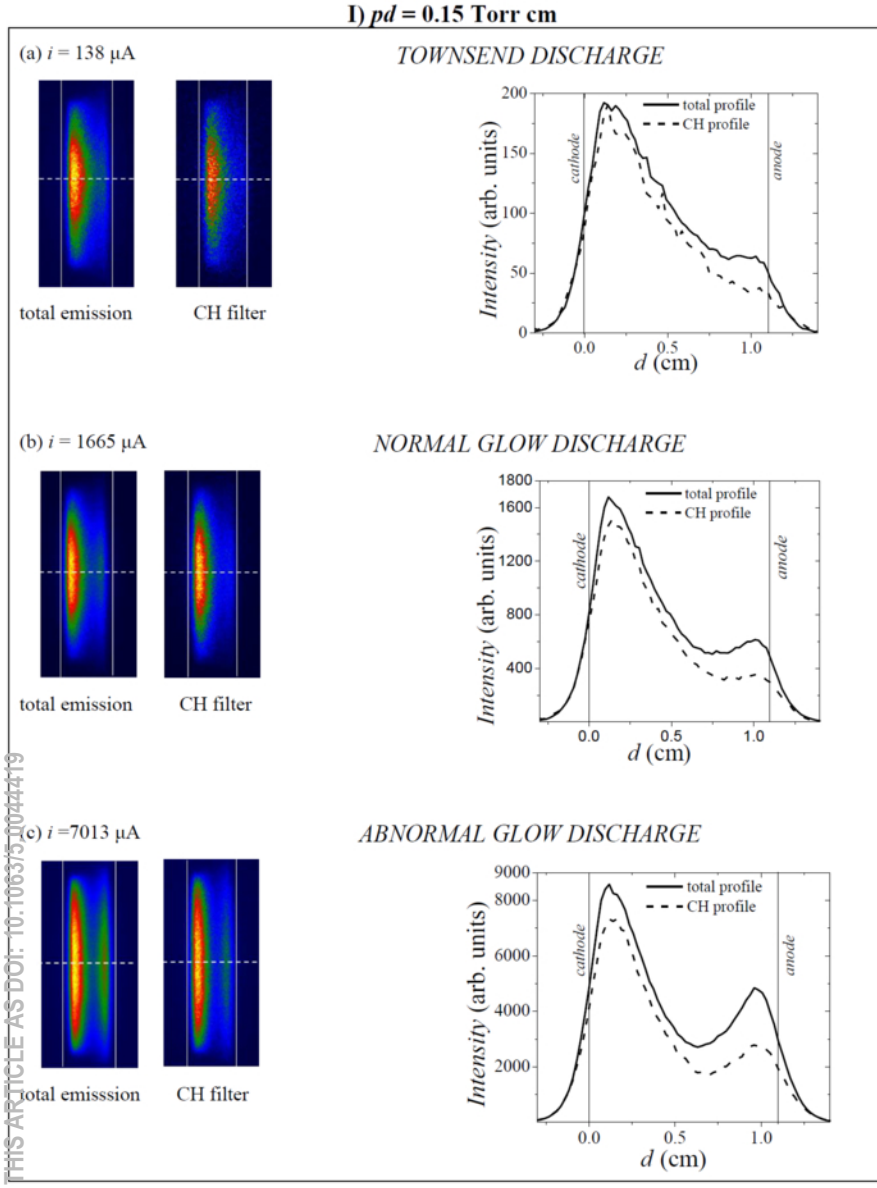

Journal of Applied Physics

AIP Publishing

PLEASE CITE THIS ARTICLE AS DOI: 10.1063/5.0044419

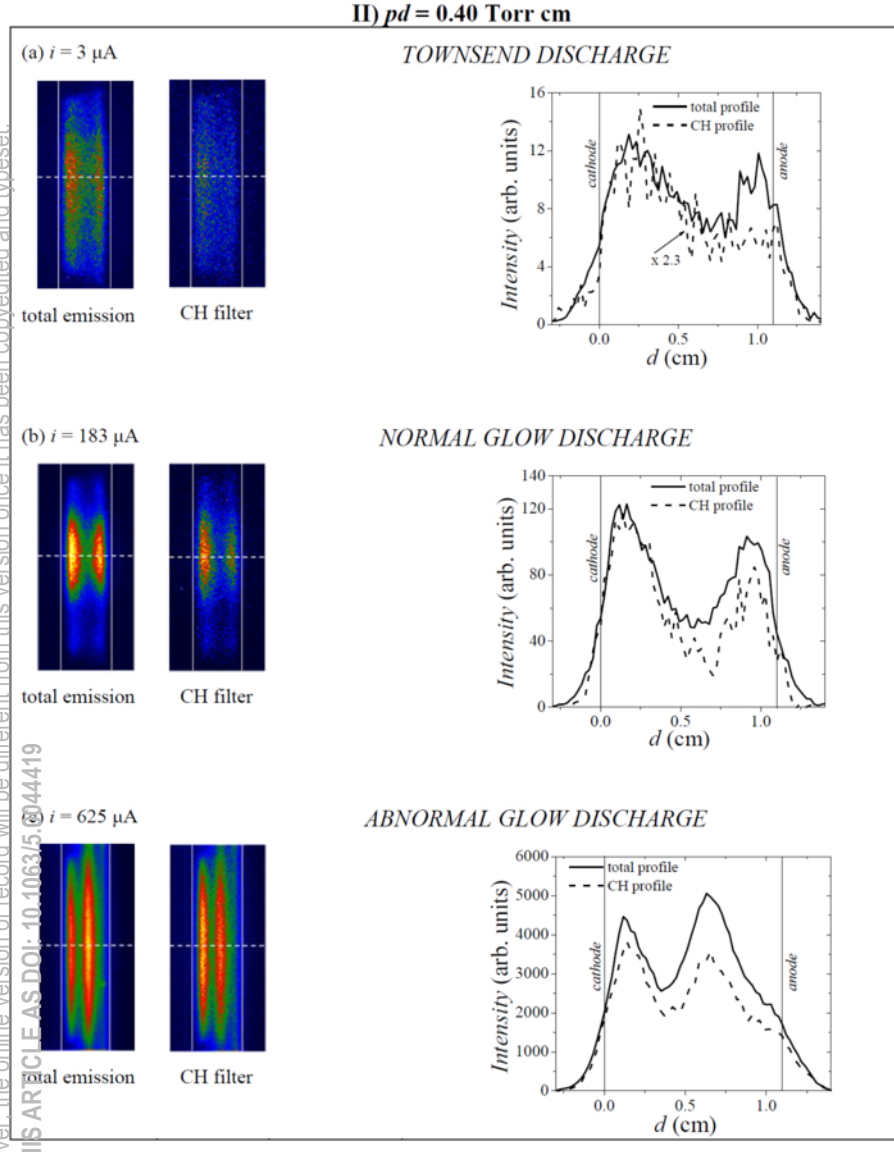

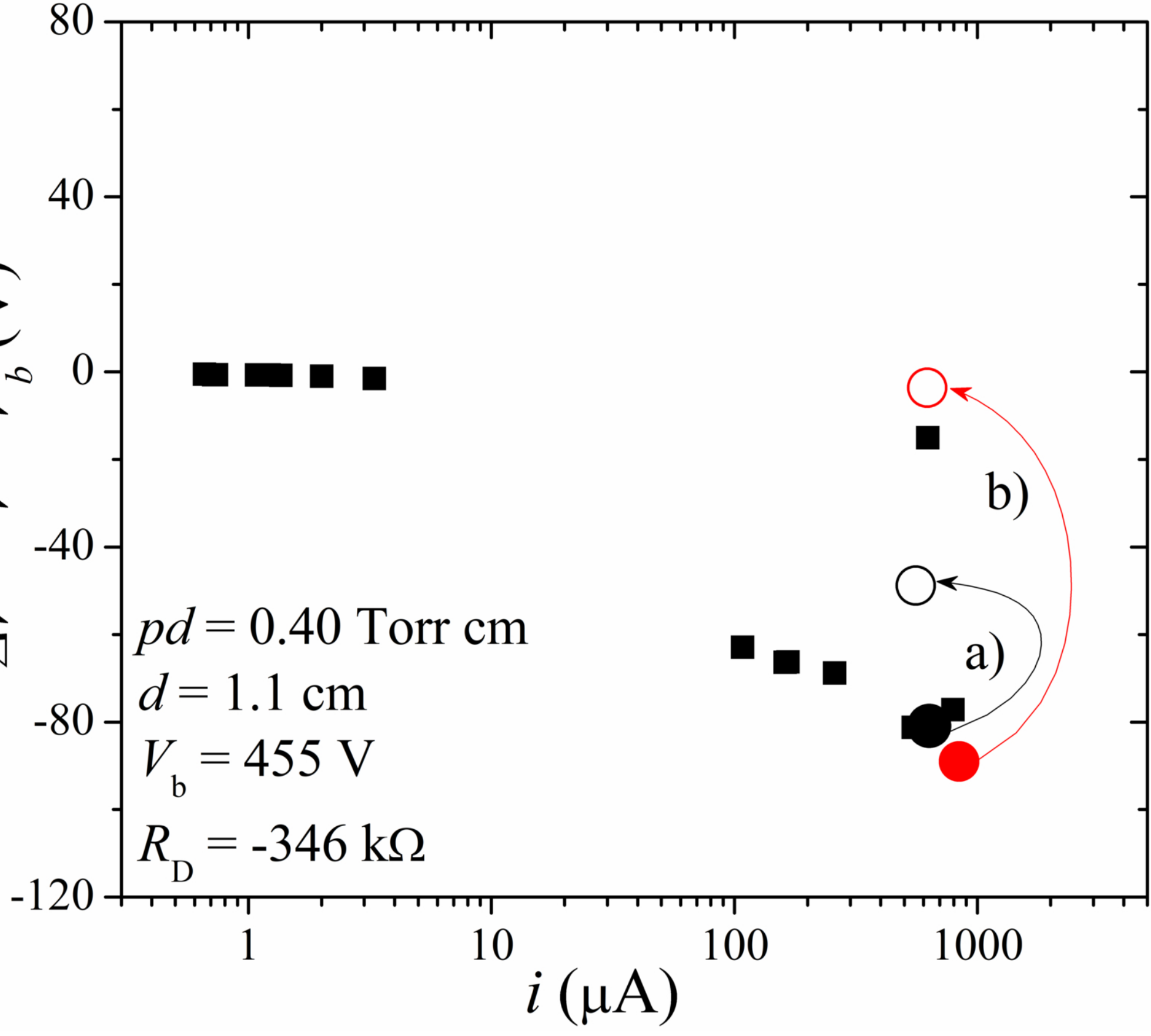

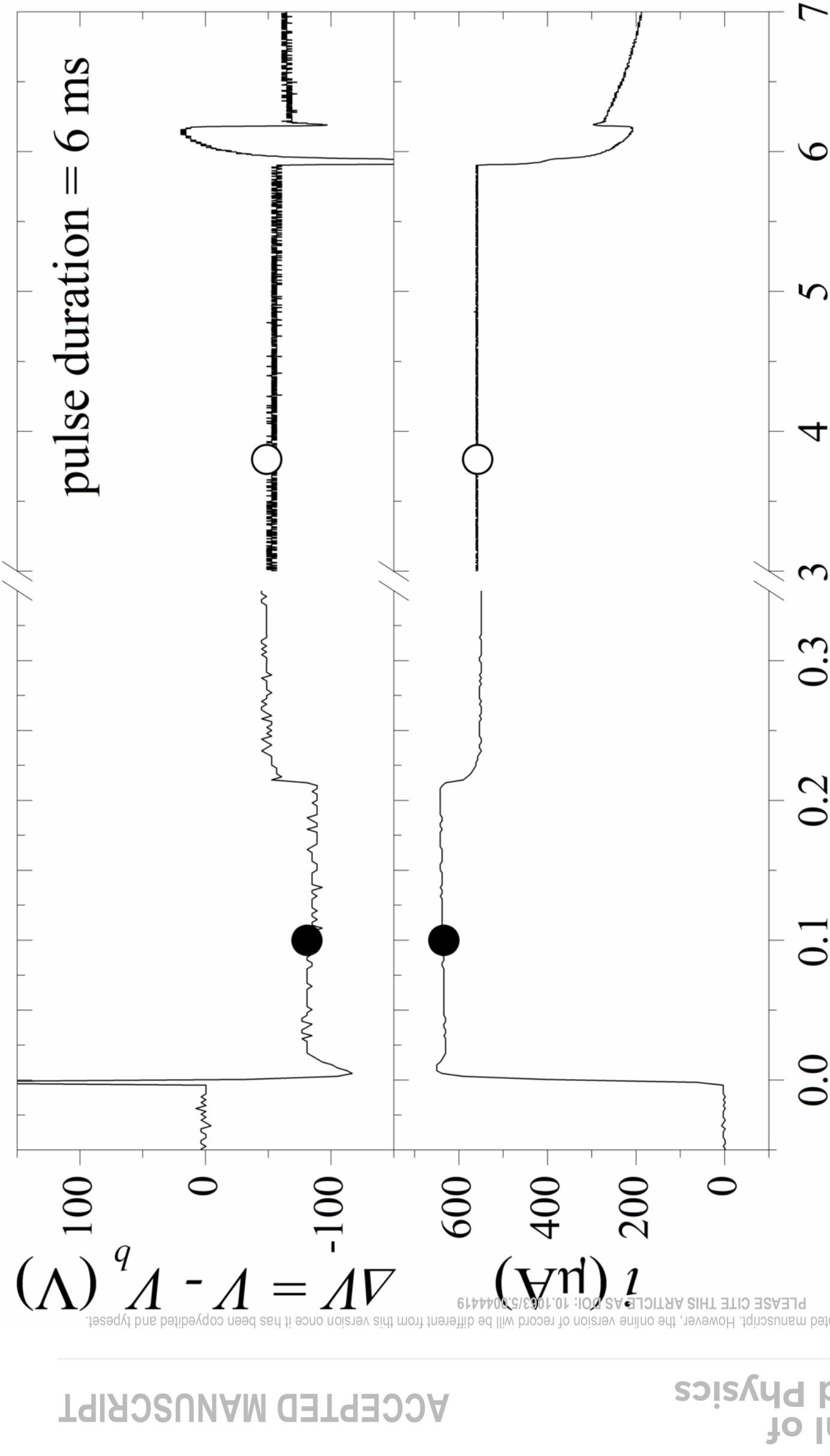

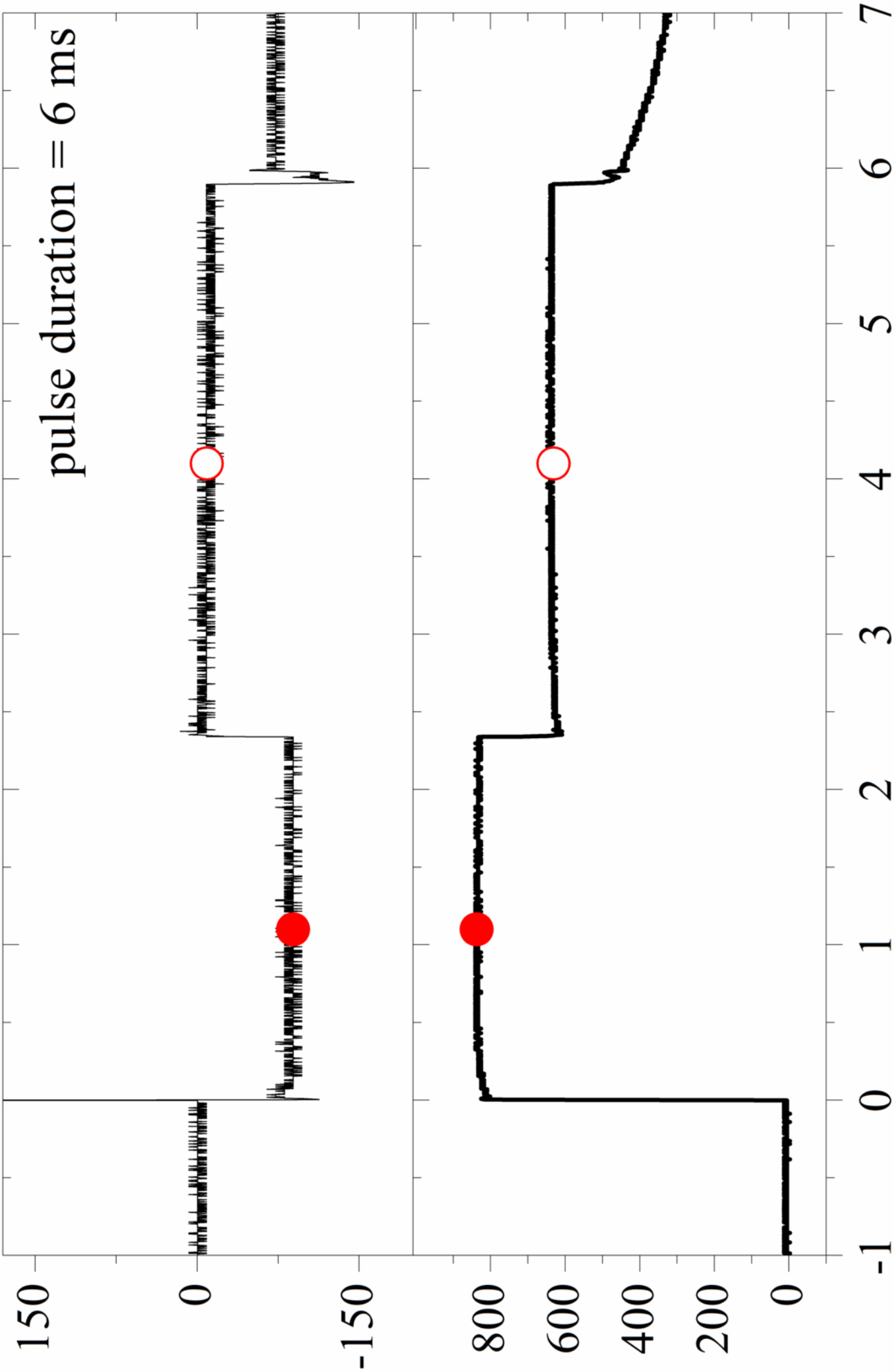

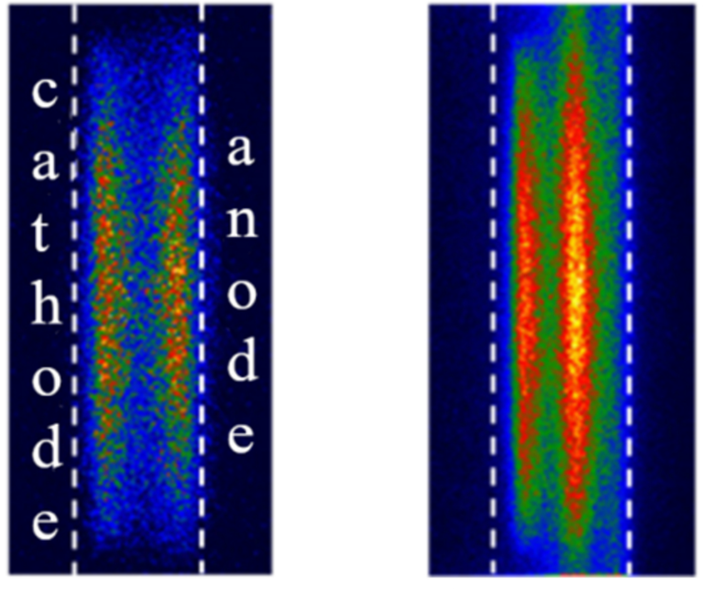

before the step after the step

a) obtained by integrating the visual spectrum

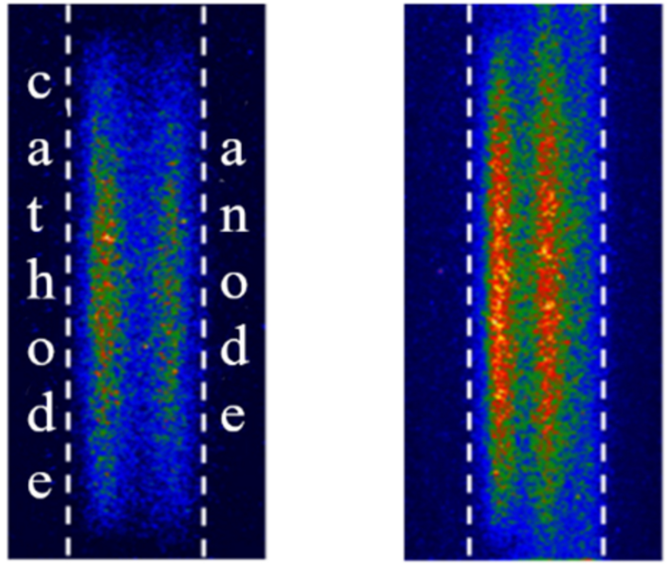

before the step after the step

b) with optical filter for CH band

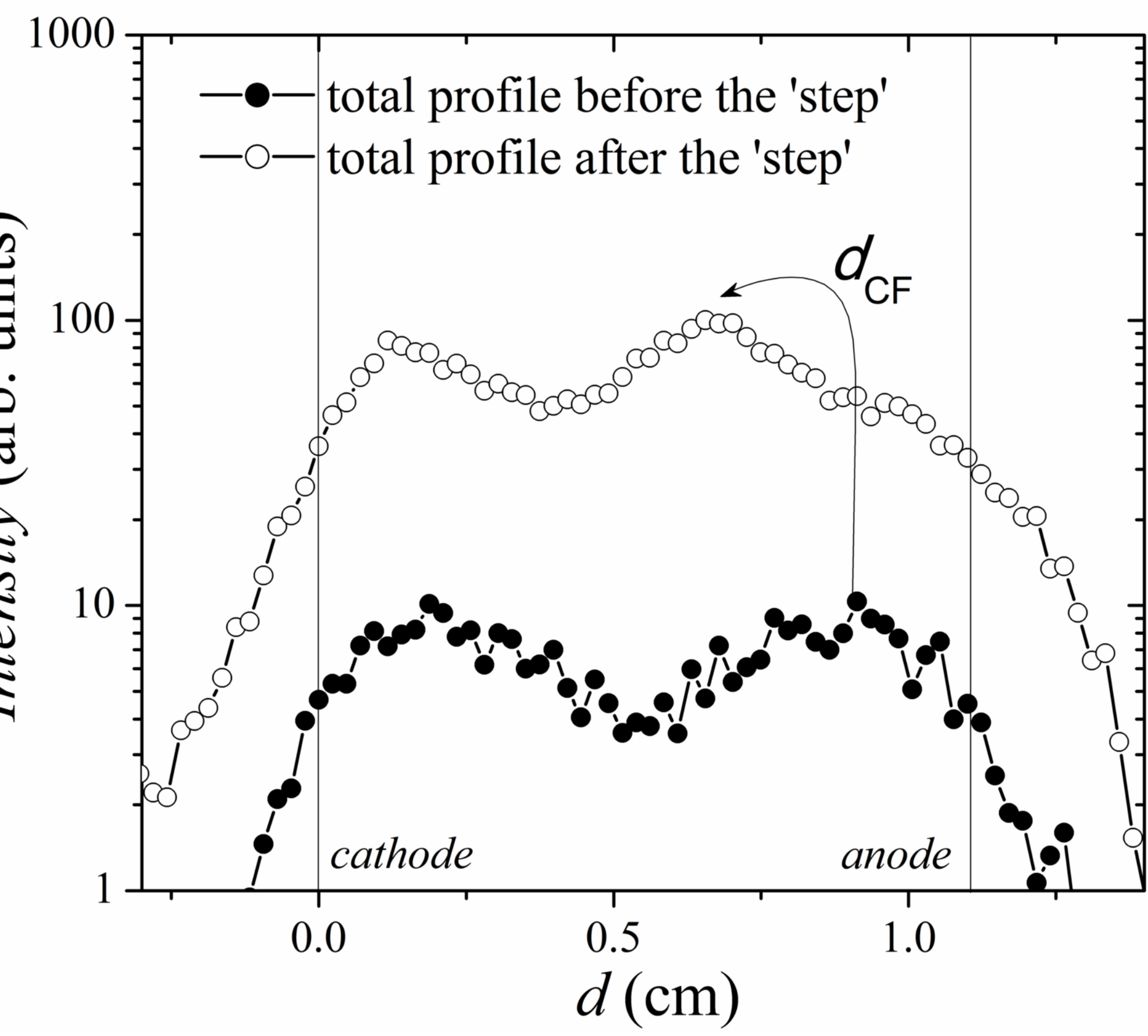

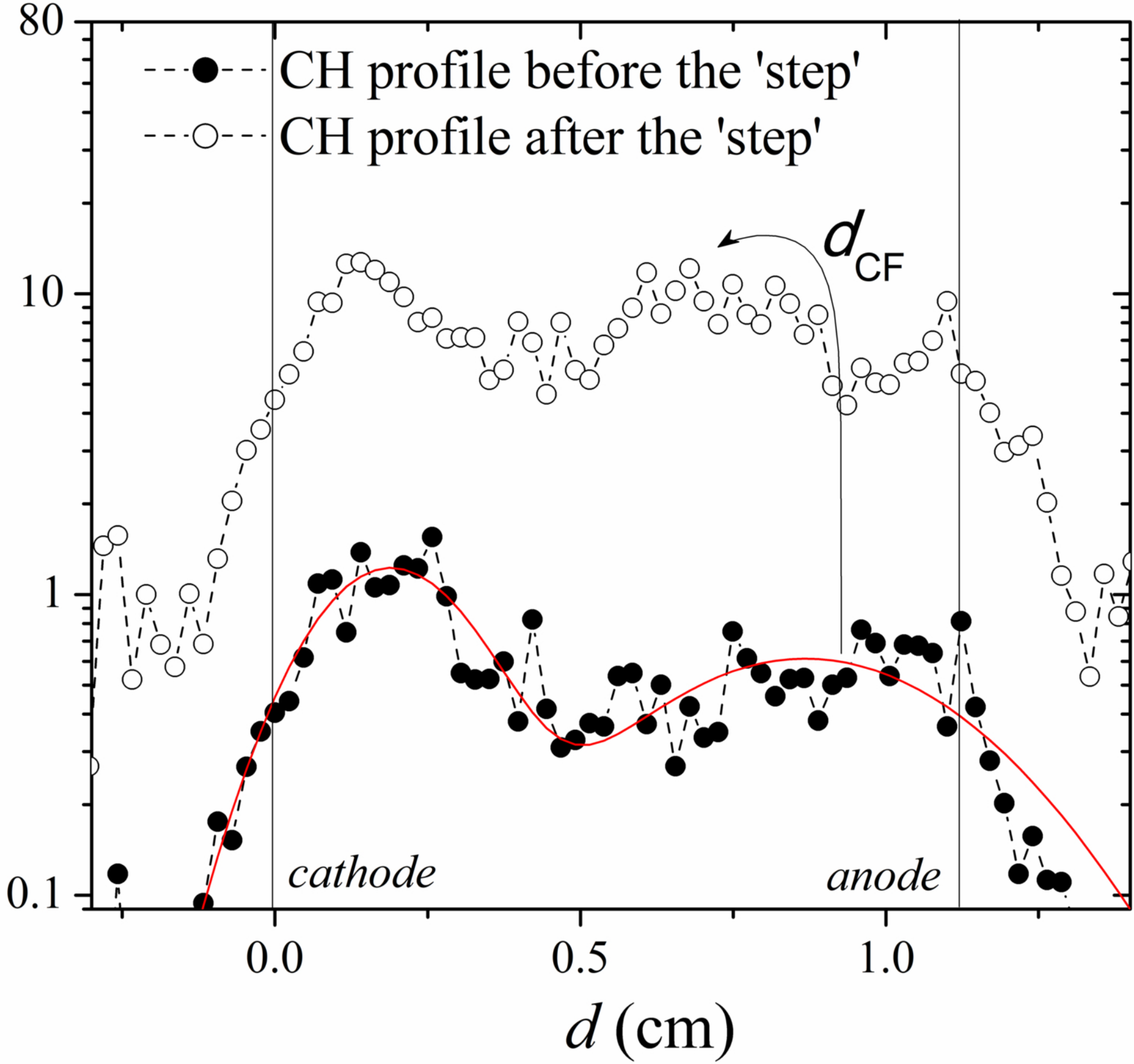

Journal of Applied Physics